Published in final edited form as:
Eur J Mech B Fluids. 2012 ; 35: 20–24. doi:10.1016/j.euromechflu.2012.01.013.

On the three-dimensional vortical structure of early diastolic flow in a patient-specific left ventricle

Trung Bao Le[a] and **Fotis Sotiropoulos**[a,*]

Trung Bao Le: lebao002@umn.edu; Fotis Sotiropoulos: fotis@umn.edu

[a]St. Anthony Falls Laboratory, Department of Civil Engineering, University of Minnesota, Minneapolis, MN, USA

Abstract

We study the formation of the mitral vortex ring during early diastolic filling in a patient-specific left ventricle using direct numerical simulation. The geometry of the left ventricle is reconstructed from Magnetic Resonance Imaging (MRI). The heart wall motion is modeled by a cell-based activation methodology, which yields physiologic kinematics with heart rate equal to 52 beats per minute. We show that the structure of the mitral vortex ring consists of the main vortex ring and trailing vortex tubes, which originate at the heart wall. The trailing vortex tubes play an important role in exciting twisting circumferential instability modes of the mitral vortex ring. At the end of diastole, the vortex ring impinges on the wall and the intraventricular flow transitions to a weak turbulent state. Our results can be used to help interprete and analyze three-dimensional *in–vivo* flow measurements obtained with MRI.

Keywords

vortex ring; intraventricular flow; patient-specific modeling

1. Introduction

Diastolic dysfunction [1] is an important contributor to heart disease and has been studied extensively in the past. Recent advancements in non-invasive technologies have enabled the use of imaging modalities for diagnosing left heart dysfunction [2, 3] but a major research challenge is to utilize such images to develop strategies for reliable diagnosis of heart disease [4, 5, 6]. Critical prerequisite for achieving this objective is to establish quantitative links between intraventricular flow patterns and cardiac disease [4, 7, 8, 6].

The diastolic flow has been shown to be dominated by the evolution of the mitral vortex ring (MVR) [9, 4] during early diastolic filling. It is now well understood that upon its formation the MVR evolves into a large asymmetrical vortical structure at the end of diastole, which occupies almost the entire left ventricular (LV) chamber [10, 11]. Various characteristics of the MVR have been shown to be linked with different types of cardiac diseases [4, 12, 7] and its formation, propagation speed, trajectory and impingement on the heart wall have all

*Corresponding author at: Saint Anthony Falls Lab., Dept. Civil Engineering, University of Minnesota, 2 Third Ave SE, Minneapolis, MN 55414. Tel: +1 612 624 2022.

been identified as clinically important phenomena [4, 13, 14]. Therefore, understanding the three-dimensional structure of the MVR is essential for analyzing and interpreting the flow patterns observed *in–vivo*.

In most previous studies [4, 8, 15, 7], the MVR is assumed to be of an axisymmetric circular vortex ring. Recent *in–vivo* measurement [3], however, have shown that the MVR deviates considerably from an axisymmetric ring and is characterized by continuous variation of its core size along its circumference. Furthremore, numerical simulations [11, 14] have shown that the ring deforms and impinges on the posterior wall before it breaks down into small scale structures. Our recent work [16] on vortex ring formation in impulsively-driven flows through inclined nozzles has shown that the vortex ring forming in such cases exhibits similar circumferential core size variation as the MVR but also evolves to become topologically complex with secondary vortex tubes emerging and interacting with the primary vortical structure. Computational studies in idealized LV chambers [17, 18] have also indicated that the MVR has a complex three-dimensional structure with the presence of secondary trailing vortex tubes. The main vortex ring has asymmetrical structure and its propagation speed varies continuously along its circumference [17].

In this work, we investigate the formation and evolution of the mitral vortex ring during early diastolic filling. We carry out high-resolution direct numerical simulation to simulate the diastolic phase of blood flow in an anatomic LV chamber at physiologic conditions with the wall motion simulated via a lumped electrophysiologic model. We clarify the three-dimensional structure of the MVR and discuss the potential clinical implications of our findings.

2. Material and methods

The left heart geometry

We reconstruct the anatomic left heart geometry from MRI data of a healthy subject. The data was provided to us by the Georgia Institute of Technology Cardiovascular Fluid Mechanics Laboratory. The aortic and mitral valve, coronary and carotid arteries as well as one part of the left atrium are removed from the original anatomy. The final geometry is shown in Fig. 1.

With reference to Fig. 1, the values for the various geometrical parameters of our LV model are as follows: the LV long and short axes lengths are $L = 80$ mm and $D_L = 47$ mm, respectively; the mitral annulus diameter is $D_M = 37$ mm; and the mitral valve is assumed to open throughout diastole with mitral orifice diameter of $D = 29$ mm as shown in Fig. 1.

The LV kinematics model

To model the LV kinematics we use the cell-based electric excitation metholodology. The approach follows lumped-type parameter models [19, 20, 21, 22], which, nevertheless, is able to reproduce the physiological features of the LV kinematics. The model is based on the following assumptions: 1) Only the LV moves. The atrium and the LV base remain stationary in the cardiac cycle; 2) Only the endocardium is modeled as the wall surface. The endocardium surface is discretized with an unstructured grid with material nodes as shown in Fig. 2. Each material node is assumed to represent one endocardium cell; and 3) The response of the endocardium cell to the cardiac electrical stimulation is assumed to be a function of a time-dependent potential $p_f(t)$.

Let $\vec{x_j}=\vec{x_j}(t)$ be the instantaneous position vector of the j^{th} endocardium cell. In cylindrical coordinate system $\vec{x_j}=\vec{x_j}(r,\theta,z)$ in Fig. 1, $\vec{x_j}$ can be decomposed into its components expressed:

$$\vec{v_j}(t)=\frac{d\vec{x_j}}{dt}=v_j^r(t)\vec{i}_r+v_j^\theta(t)\vec{i}_\theta+v_j^z(t)\vec{i}_z \quad (1)$$

where v_j^r, v_j^θ, and v_j^z are the radial, tangential and axial velocity components, respectively. The vector $\vec{i_r}$, $\vec{i_\theta}$, and $\vec{i_z}$ are the radial, tangential and axial unit vector, respectively. We model the instantaneous velocity magnitude $v_j=|\vec{v_j}(t)|$ a function of the potential $p_j(t)$ as follows.

The velocity magnitude is decomposed as the product of a time-dependent wave propagation part Ω [23] and a spatial distribution part ℑ:

$$v_j(t)=\Omega(\vec{x_j},t)\Im(\vec{x_j}) \quad (2)$$

We assume that $\Im(\vec{x_j},t)$ is a function of the radial (r_j) and longitudinal (z_j) coordinates [19]:

$$\Im(\vec{x_j})=\left(\frac{2r_j}{D_L}\right)^2\left(\frac{z_j}{L}\right)^{1.5} \quad (3)$$

The wave propagation part $\Omega(\vec{x_j},t)$ is modelled as the product of a local, time-dependent part $E_j(t)$ and a wave-propagation part $S(\vec{x_j},t)$:

$$\Omega(\vec{x_j},t)=E_j(t)S(\vec{x_j},t) \quad (4)$$

E_j is assumed to be a function of the time-dependent potential p_j, i.e. $E_j(t) = E[p_j(t)]$. The specific functional form of E_j is prescribed as the equilibrium solution of the dimensionless form of the FitzHugh-Nagumo system of equations, as follows [23, 24, 25]:

$$E_j(t)=c_1 p_j(t)\,[p_j(t)-c_0]\,[p_j(t)-1]+c_2\,[p_j(t)-1]\,[1-\exp(-c_3 p_j(t))] \quad (5)$$

with $p_j(t)$ and the model constants c_0, c_1, c_2 and c_3 prescribed as part of the calibration of the model (see below).

To account for the spatial propagation of the mechanical response wave front [26, 27], the S term in Eq. 4 is modeled as a sine wave function [20, 26] with scaling frequency factor f_s and phase lag ϕ, as follows:

$$S(\vec{x_j},t)=\kappa\sin\left(2\pi f_s\frac{t}{T}-\frac{z_j}{L}+\phi\right) \quad (6)$$

where κ is the parameter of the model while T is the heart beat cycle.

Eqs. 3, 4, 5, and 6 above complete the model for the instantaneous velocity magnitude $v_j(t)$ of each endocardium cell. The final step before the three-dimensional LV wall configuration can be updated in time by integrating Eq. 1 is to define the three components of the velocity

vector. To do so, we distribute the known velocity magnitude v_j along the three cylindrical coordinate directions as follows:

$$\begin{aligned} v_j^r(t) &= \alpha v_j(t) \\ v_j^\theta(t) &= \beta v_j(t) \\ v_j^\theta(t) &= \gamma v_j(t) \end{aligned} \tag{7}$$

where α, β and γ are parameters of the model satisfying $\alpha^2 + \beta^2 + \gamma^2 = 1$. The relative nagnitude of these three parameters is specified using input from MRI data [28] to mimic the observed in vivo relative ratios of the three velocity components of the LV wall.

We calibrate the model parameters (i.e c_0, c_1, c_2 etc.) and the functional form for $p(t)$ to ensure that the resulting temporal variation of the LV volume $V = V(t)$, dV/dt, agrees with reported values in the literature [29, 30].

The numerical method and computational details

Blood is simulated as an incompressible, Newtonian fluid with dynamic viscosity of $\nu = 3.35 \times 10^{-6} m^2/s$ and thus its motion is governed by the unsteady, three-dimensional Navier-Stokes equations. The moving LV surface is discretized with an unstructured grid (see Fig. 2) and is immersed in a background, stationary, curvilinear grid of size 201×201×193 (see Fig. 2). The LV surface is treated as a sharp interface using the Curvilinear Immersed Boundary (CURVIB) method [31, 32]. The governing equations are discretized via second-order accurate finite-difference formulas and integrated in time using an efficient, second-order accaurate fractional-step method [31, 32]. The cardiac cycle in our simulation is $T = 1.15 s$, corresponding to a physiologic heart rate of 52 beats per minute, and the computational timestep is set to be $\Delta t = 0.426\ ms$.

The mitral inflow waveform used in the simulation, which is indicative of the LV wall kinematics obtained from our model, is shown in Figure 3. This waveform is used to specify the time-dependent blood flow flux from the left atrium to the LV chamber as boundary condition at the mitral orifice $Q_m = Q_m(t)$. We assume uniform flow distribution at the mitral orifice, which is broadly similar to the natural conditions during diastole [33, 34]. Since the simulations reported herein are carried out only during diastole, the aortic valve is kept fully closed by setting the flow rate through the aorta equal to zero at all times. Finally, the time-dependent LV wall motion is prescribed as input to the simulation from the previously described cell-activation model and is used to drive the LV blood flow through the no-slip and no-flux boundary conditions that are imposed for the velocity field at the LV wall.

3. Results and discussions

The calculated LV wall kinematics that emerge from the cell-activation model described above is well within the physiologic range as indicated by several global cardiac parameters shown in Table 2. The corresponding diastolic volume flow rate curve is shown in Fig. 3. Note that the flow rate has two distinct positive peaks, which correspond to the E-wave and A-wave peaks, respectively. The E-wave peak is the instant in time when the flow rapidly fills the LV chamber from the left atrium as the mitral valves opens. The A-wave peak results from the active pumping of atrium to the left ventricle [1].

During the diastolic phase the intraventricular flow is dominated by the filling of blood flow from the left atrium into the left ventricular chamber. At initial phase of the E-wave filling, we observe the existence of a large well-defined vortex ring formed at the edge of the mitral orifice as seen in Fig. 4a. Since the mitral orifice has a circular shape, the mitral vortex ring

has the initial donut-shape vorticity distribution around the main's ring circumference. After the E-wave, this vortex ring is fully formed and propagates toward the LV apex.

The calculated three-dimensional structure of the diastolic vortical structures are visualized in Fig. 4 in terms of an instantaneous iso-surface of the vorticity magnitude. As seen in Fig. 4a, the MVR has a variable core diameter and begins to interact with the basal geometry shortly after it forms. This interaction causes vorticity to be extracted from the wall and induces the formation of secondary vortex tubes, denoted as trailing vortex tubes, that grow from the wall and wrap around the primary ring clearly on during diastole as shown in Fig. 4a. Moreover, the ring starts to become inclined and propagates toward the posterior wall. As shown in Figures 4b and b, the second phase of the MVR evolution is characterized by the stretching and elongation of the secondary vortex tubes, which, while remaining attached to the wall, are seen to wrap around the core of the MVR giving rise to the growth of twisting instabilities along the ring core. As the MVR advances toward the apex, both the twisting of the secondary vortex tubes around the MVR core as well as the twisting of the MVR core itself intensify as seen in Fig. 4c only. At the end of diastole and as seen in Fig. 4d, the MVR impinges on the LV wall and begins to break down into small-scale structures while the trailing secondary vortex tubes remain coherent. The same figure also shows the formation of the A-wave vortex ring just downstream of the mitral orifice.

Overall Fig. 4 underscores the highly three-dimensional structure of the MVR. It is worth noting, however, that the emerging rich topology of the vortical structure is, as one would anticipate, not immediately apparent when plotting two-dimensional velocity vectors on a plane through the center of the LV chamber as shown in Fig. 5. Such two dimensional plots reveal flow patterns that are quite similar to those observed in recent in vivo measurements with MRI [10, 2, 3]. They clearly illustrate the asymmetry of the MVR and the growth of a large clock-wise rotating vortex occupying almost the entire LV chamber but naturally cannot provide any insights into the three-dimensional complexity of the flow.

The topology of the MVR we observe in our simulations with the secondary vortex tubes wrapping around its core has also been observed in previous numerical simulations using idealized LV models [17]. In such models, the secondary vortex tubes extend upstream of the mitral orifice and are orthogonal to the main LV axis. Our results are consistent with the previous idealized study [17] and clearly show that the existence of the secondary vortex tubes is the direct consequence of the interaction between the MVR and the LV wall. These secondary tubes do not play a direct role in the MVR's break up during late diastole, which occurs when the MVR impinges on the LV wall. Such structures, however, intensify the topological complexity of the MVR as tend to attenuate the twisting instabilities that grow around its circumference.

The three-dimensional topology of the MVR as emerges from our simulations shares several common characteristics with that of a vortex ring emerging as the flow is driven impulsively through a cylindrical nozzle with an inclined orifice into a stagnamt ambient fluid [16]. We have recently shown [16] that for such asymmetric nozzle orifice, the vortex ring formation deviates considerably from that of a perfectly circular ring. The flow is characterized by the growth of secondary vortex tubes due to wall-vortex and vortex-vortex interaction, the wrapping of these tubes around the core of the primary ring, and the growth of complex, twisting instability modes [16]. In the present case the orifice geometry is cylindrical and symmetric but the surrounding LV chamber is three-dimensional. More specifically, the flow from the mitral orifice near the aortic side has more space available to grow and entrain fluid into the MVR as opposed to the flow near the oposite side of the LV. This geometric asymmetry sets up a situation broadly similar to that observed in inclined nozzles where entrainment is maximized near the short lip of the nozzle. As shown in [16], the geometry

induced asymmetry of the vortex ring from an inclined nozzle is ultimately responsible for the growth of complex secondary structures and twisting instability modes.

The deformation of the MVR documented in our simulations is also consistent with other recent computational works [11] and *in-vivo* measurement [2, 35]. Our results in Fig. 4a–d show that the stretching and impingement of the MVR on the posterior wall is the reason for setting up the clockwise rotating flow observed *in–vivo*. Our simulations have also shown that the MVR exhibits twisting instabilities along its core before it impinges on the LV wall. Its breakdown into a turbulent-like state, as shown in Fig 4d, also agrees well with findings from idealized models of [17].

4. Conclusions

We study the formation of the MVR in patient-specific anatomy using direct numerical simulation. Our results reveal a complex, three-dimensional vortical structure consisting of the main ring and pairs of secondary vortex tubes wrapping around the main ring's core. The trailing vortex tubes originate from the heart wall and strtech and twist around the MVR's circumference, inducing twisting instabilities to grow and propagate along the ring's circumference. The impingement of the MVR of the LV wall and its subsequent breakup leads to a turbulent-like state at the end of diastole.

In our work the dynamics of the mitral valve is not simulated and thus its effect on the overall LV flow patterns is not considered. However, *in–vivo* data [36, 34, 3] suggest that such effect is rather limited close to the mitral orifice and does not extend far from the mitral valve tips. Therefore, the conclusions of our work can be useful for understanding the MVR topology *in–vivo* and facilitating the interpretation of MRI imaging data.

Acknowledgments

This work was supported by NIH Grant RO1-HL-07262 and the Minnesota Supercomputing Institute. We thank Ajit Yoganathan and the members of the Georgia Tech Cardiovascular Fluid Mechanics Laboratory for providing us with the anatomic LV geometry used in this study. The first author is partially supported by a fellowship from Vietnam Education Foundation.

References

1. Yellin EL, Meisner JS. Physiology of diastolic function and transmitral pressure-flow relations. Cardiology Clinics. 2000; 18:411–433. [PubMed: 10986581]
2. Eriksson J, Carlhall C, Dyverfeldt P, Engvall J, Bolger A, Ebbers T. Semi-automatic quantification of 4d left ventricular blood flow. Journal of Cardiovascular Magnetic Resonance. 2010; 12:9. [PubMed: 20152026]
3. Markl M, Kilner P, Ebbers T. Comprehensive 4d velocity mapping of the heart and great vessels by cardiovascular magnetic resonance. Journal of Cardiovascular Magnetic Resonance. 2011; 13:7. [PubMed: 21235751]
4. Gharib M, Rambod E, Kheradvar A, Sahn DJ, Dabiri JO. Optimal vortex formation as an index of cardiac health. Proceedings of the National Academy of Sciences. 2006; 103:6305–6308.
5. Ghosh E, Shmuylovich L, Kovcs SJ. Vortex formation time-to-left ventricular early rapid filling relation: model-based prediction with echocardiographic validation. Journal of Applied Physiology. 2010; 109:1812–1819. [PubMed: 20864560]
6. Zhong L, Su Y, Gobeawan L, Sola S, Tan RS, Navia JL, Ghista DN, Chua T, Guccione J, Kassab GS. Impact of surgical ventricular restoration on ventricular shape, wall stress, and function in heart failure patients. American Journal of Physiology - Heart and Circulatory Physiology. 2011; 300:H1653–H1660. [PubMed: 21357513]
7. Kheradvar A, Houle H, Pedrizzetti G, Tonti G, Belcik T, Ashraf M, Lindner JR, Gharib M, Sahn D. Echocardiographic particle image velocimetry: A novel technique for quantification of left

ventricular blood vorticity pattern. Journal of the American Society of Echocardiography. 2010; 23:86–94. [PubMed: 19836203]

8. Hong GR, Pedrizzetti G, Tonti G, Li P, Wei Z, Kim JK, Baweja A, Liu S, Chung N, Houle H, Narula J, Vannan MA. Characterization and Quantification of Vortex Flow in the Human Left Ventricle by Contrast Echocardiography Using Vector Particle Image Velocimetry. J Am Coll Cardiol Img. 2008; 1:705–717.
9. Kim WY, Walker PG, Pedersen EM, Poulsen JK, Oyre S, Houlind K, Yoganathan AP. Left ventricular blood flow patterns in normal subjects: A quantitative analysis by three-dimensional magnetic resonance velocity mapping. Journal of the American College of Cardiology. 1995; 26:224–238. [PubMed: 7797756]
10. Kilner PJ, Yang G-Z, Wilkes AJ, Mohiaddin RH, Firmin DN, Yacoub MH. Asymmetric redirection of flow through the heart. Nature. 2000:404.
11. Schenkel T, Malve M, Reik M, Markl M, Jung B, Oertel H. Mri-based cfd analysis of flow in a human left ventricle: Methodology and application to a healthy heart. Annals of Biomedical Engineering. 2009; 37:503–515. [PubMed: 19130229]
12. Doenst T, Spiegel K, Reik M, Markl M, Hennig J, Nitzsche S, Beyersdorf F, Oertel H. Fluid-dynamic modeling of the human left ventricle: Methodology and application to surgical ventricular reconstruction. The Annals of Thoracic Surgery. 2009; 87:1187–1195. [PubMed: 19324149]
13. Watanabe H, Sugiura S, Hisada T. The looped heart does not save energy by maintaining the momentum of blood flowing in the ventricle. American Journal of Physiology - Heart and Circulatory Physiology. 2008; 294:H2191–H2196. [PubMed: 18326797]
14. Krittian S, Janoske U, Oertel H, Bhlke T. Partitioned fluidsolid coupling for cardiovascular blood flow. Annals of Biomedical Engineering. 2010; 38:1426–1441. [PubMed: 20058187]
15. Faludi R, Szulik M, D'hooge J, Herijgers P, Rademakers F, Pedrizzetti G, Voigt JU. Left ventricular flow patterns in healthy subjects and patients with prosthetic mitral valves: An in vivo study using echocardiographic particle image velocimetry. J Thorac Cardiovasc Surg. 2010; 139:1501–1510. [PubMed: 20363003]
16. Le TB, Borazjani I, Kang S, Sotiropoulos F. On the structure of vortex rings from inclined nozzles. Journal Fluid Mechanics. 2011
17. Domenichini F, Pedrizzetti G, Baccani B. Three-dimensional filling flow into a model left ventricle. Journal of Fluid Mechanics. 2005; 539:179–198.
18. Domenichini F, Querzoli G, Cenedese A, Pedrizzetti G. Combined experimental and numerical analysis of the flow structure into the left ventricle. Journal of Biomechanics. 2007; 40:1988–1994. [PubMed: 17097665]
19. Chadwick R. Mechanics of the left ventricle. Biophysical Journal. 1982; 39:279–288. [PubMed: 7139027]
20. Beyar R, Sideman S. A computer study of the left ventricular performance based on fiber structure, sarcomere dynamics, and transmural electrical propagation velocity. Circ Res. 1984; 55:358–375. [PubMed: 6467528]
21. Beyar R, Sideman S. The dynamic twisting of the left ventricle: A computer study. Annals of Biomedical Engineering. 1986; 14:547–562. [PubMed: 3826804]
22. Kovacs SJ, Mcqueen DM, Peskin CS. Modelling cardiac fluid dynamics and diastolic function. Philosophical Transactions of the Royal Society of London. Series A: Mathematical, Physical and Engineering Sciences. 2001; 359:1299–1314.
23. Nash MP, Panfilov AV. Electromechanical model of excitable tissue to study reentrant cardiac arrhythmias. Progress in Biophysics and Molecular Biology. 2004; 85:501–522. Modelling Cellular and Tissue Function. [PubMed: 15142759]
24. Panfilov A, Hogeweg P. Spiral breakup in a modified fitzhugh-nagumo model. Physics Letters A. 1993; 176:295–299.
25. Aliev RR, Panfilov AV. A simple two-variable model of cardiac excitation, Chaos. Solitons and Fractals. 1996; 7:293–301.
26. Pernot M, Fujikura K, Fung-Kee-Fung SD, Konofagou EE. Ecggated, mechanical and electromechanical wave imaging of cardiovascular tissues in vivo. Ultrasound in Medicine and Biology. 2007; 33:1075–1085. [PubMed: 17507146]

27. Sengupta PP, Tondato F, Khandheria BK, Belohlavek M, Jahangir A. Electromechanical activation sequence in normal heart. Heart Failure Clinics. 2008; 4:303–314. Function Follows Form. [PubMed: 18598982]

28. Jung B, Markl M, Foll D, Hennig J. Investigating myocardial motion by MRI using tissue phase mapping. Eur J Cardiothorac Surg. 2006; 29:S150–157. [PubMed: 16563784]

29. Cheng Y, Oertel H, Schenkel T. Fluid-structure coupled cfd simulation of the left ventricular flow during filling phase. Annals of Biomedical Engineering. 2005; 33:567–576. [PubMed: 15981858]

30. Baccani B, Domenichini F, Pedrizzetti G, Tonti G. Fluid dynamics of the left ventricular filling in dilated cardiomyopathy. Journal of Biomechanics. 2002; 35:665–671. [PubMed: 11955506]

31. Ge L, Sotiropoulos F. A numerical method for solving the 3d unsteady incompressible navier-stokes equations in curvilinear domains with complex immersed boundaries. Journal of Computational Physics. 2007; 225:1782. [PubMed: 19194533]

32. Borazjani I, Ge L, Sotiropoulos F. Curvilinear immersed boundary method for simulating fluid structure interaction with complex 3d rigid bodies. Journal of Computational Physics. 2008; 227:7587–7620. [PubMed: 20981246]

33. Querzoli G, Fortini S, Cenedese A. Effect of the prosthetic mitral valve on vortex dynamics and turbulence of the left ventricular flow. Physics of Fluids. 2010; 22:041901.

34. Saber NR, Wood NB, Gosman AD, Merrifield RD, Yang GZ, Charrier CL, Gatehouse PD, Firmin DN. Progress towards patient-specific computational flow modeling of the left heart via combination of magnetic resonance imaging with computational fluid dynamics. Annals of Biomedical Engineering. 2003; 31:42–52. [PubMed: 12572655]

35. Toger J, Carlsson M, Sderlind G, Arheden H, Heiberg E. Volume tracking: A new method for quantitative assessment and visualization of intracardiac blood flow from three-dimensional, time-resolved, three-component magnetic resonance velocity mapping. BMC Medical Imaging. 2011

36. Fujimoto S, Mohiaddin RH, Parker KH, Gibson DG. Magnetic resonance velocity mapping of normal human transmitral velocity profiles. Heart and Vessels. 1995; 10:236–240. [PubMed: 8903998]

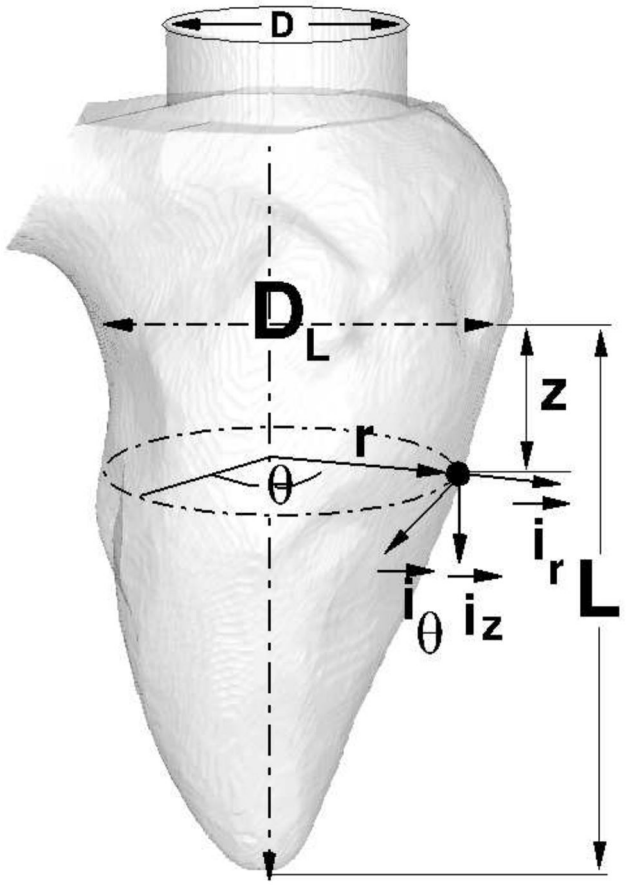

Figure 1.
The left heart model reconstructed from MRI images. (r, θ, z) is the cylindrical coordinate system defined for the LV with corresponding unit vectors $\vec{i_r}$, $\vec{i_\theta}$, and $\vec{i_z}$. L and D_L are the lengths of the long and short LV axes, respectively. At the mitral position, uniform pulsatile flow $Q_m(t)$ is specified as boundary condition as the mitral valve is assumed to be fully open during diastole. The blood flow is driven by the LV wall motion resulting from the cell-activation model. The aortic valve is fully close during diastole.

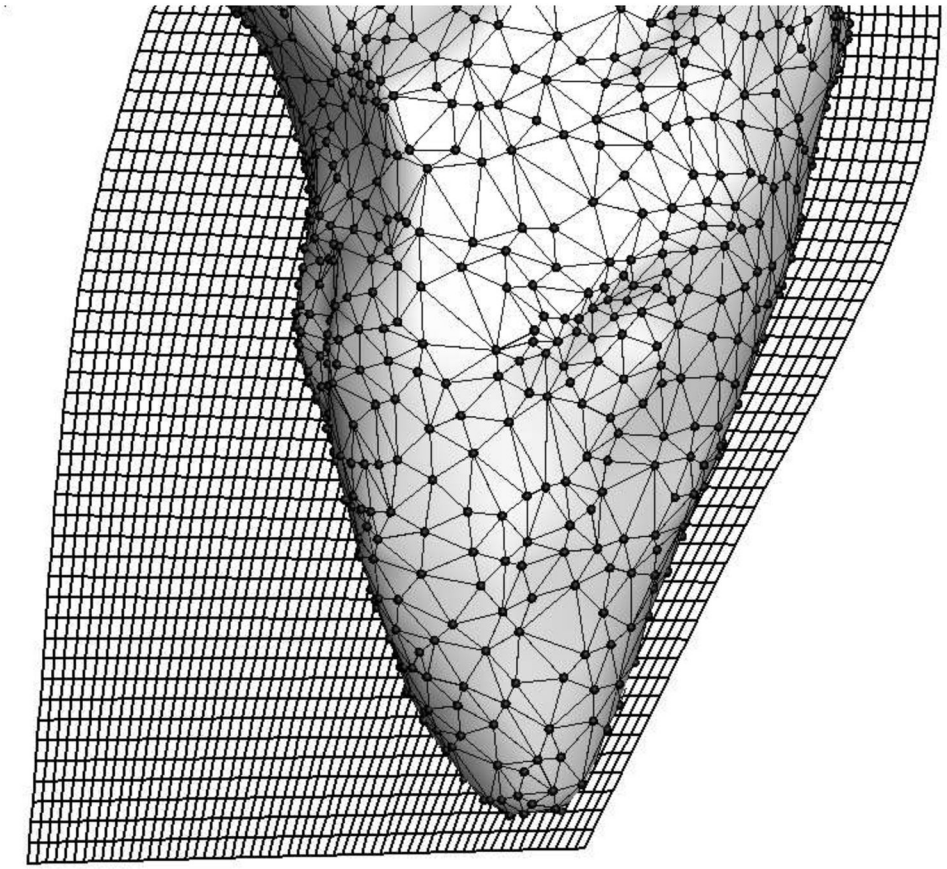

Figure 2.
The moving LV model, discretized with the unstructured grid, immersed in a background stationary curvilinear mesh as required by the CURVIB method. For clarity, the 3D background grid is shown only on the symmetry plane of the mitral orifice for every four grid line.

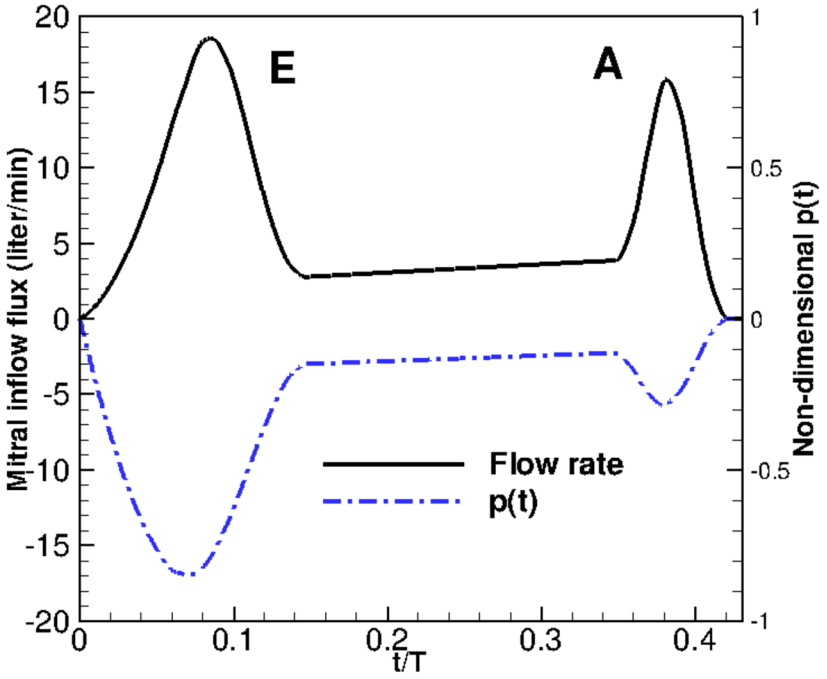

Figure 3.

The left ventricle volume rate of change $\frac{dV}{dt}$ (also the mitral inflow flux $Q_m(t)$) during diastole resulting from the cell-activation model. There are two distinct positive E-wave and A-wave peaks separated by the diastasis during diastole.

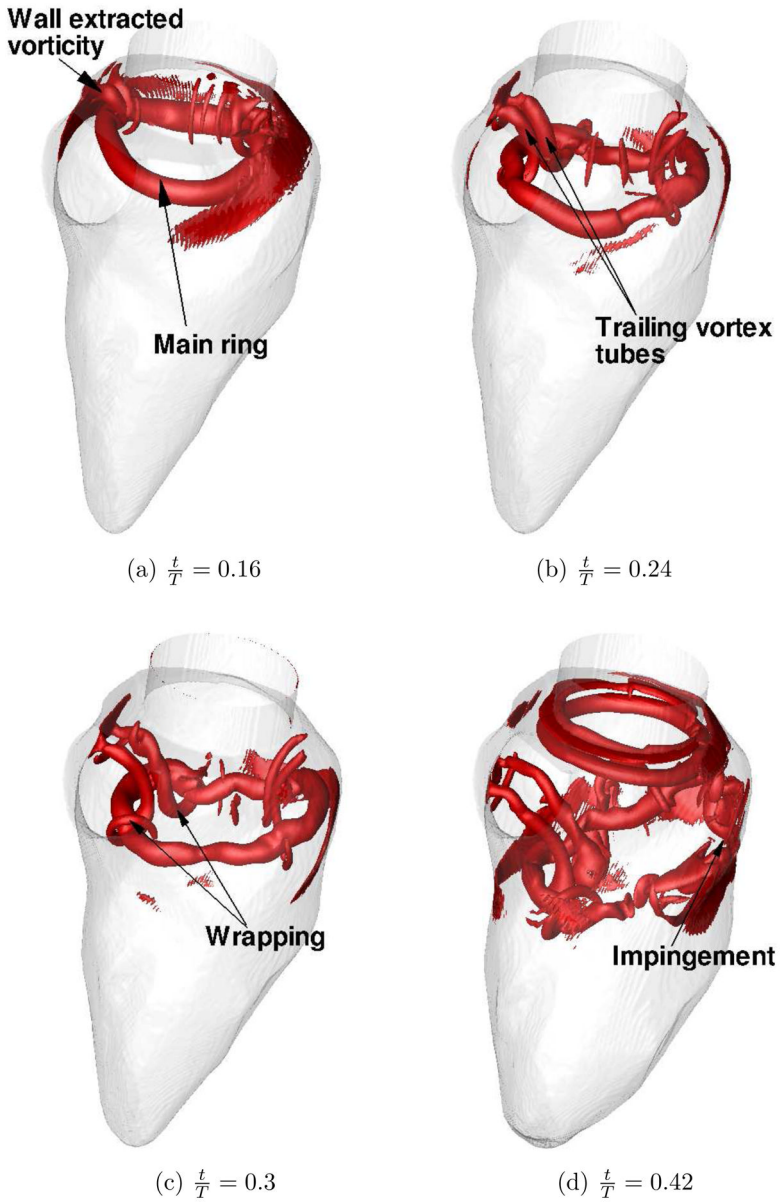

(a) $\frac{t}{T} = 0.16$ (b) $\frac{t}{T} = 0.24$

(c) $\frac{t}{T} = 0.3$ (d) $\frac{t}{T} = 0.42$

Figure 4.

The evolution of the mitral vortex ring. The flow is visualized by the non-dimensional vorticity magnitude $\frac{|\omega|D}{U}=7$. T is the cardiac cycle.

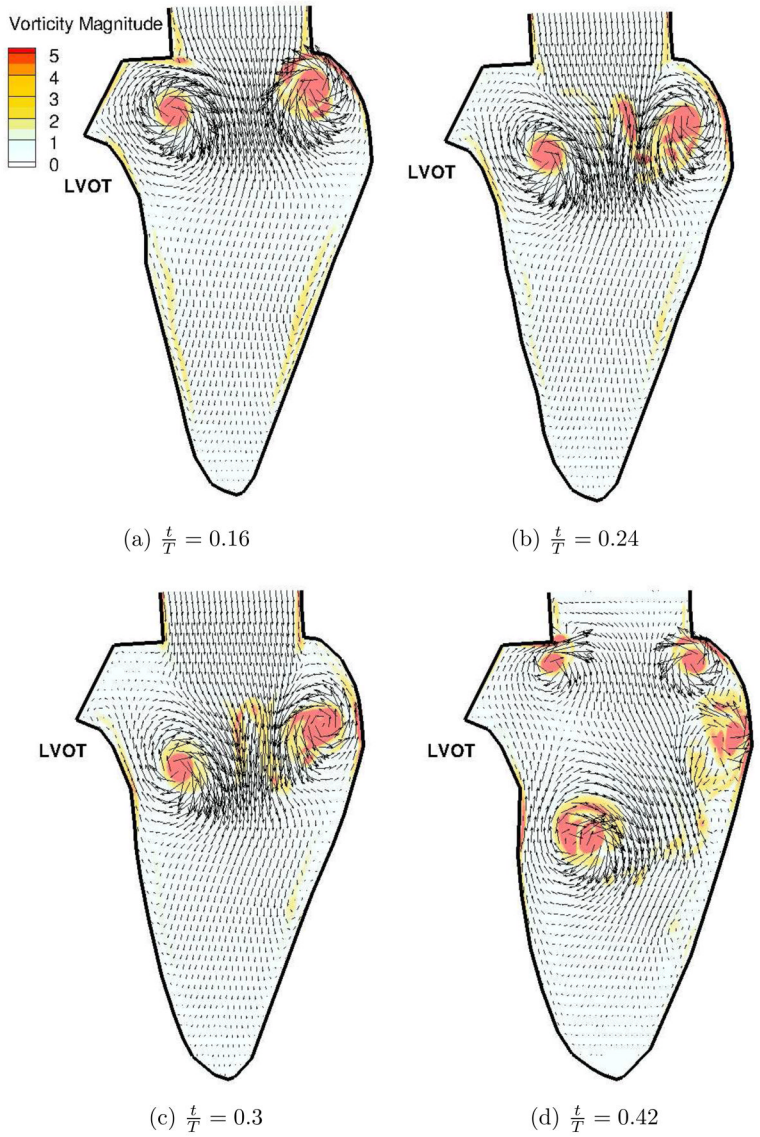

Figure 5.

The evolution of the mitral vortex ring. The flow is visualized by the velocity vectors superimposed on the contour of non-dimensional vorticity magnitude $\frac{|\omega|D}{U}$. $LVOT$ is the acronym of the Left Ventricular Outflow Tract.

Table 1

Calibrated non-dimensional parameters used in the LV kinematic model during diastole: c_0, c_1, c_2, c_3 are variables of the FitzHugh-Nagumo model; T is the cardiac cycle; f_s is the scaling frequency factor of the propagating wave front; κ is the scaling factor; α, β, γ are the distributing factors of the velocity vector along radial, tangential and axial directions, respectively (see Equation 7 for definition).

Name	Parameter
c_0	1
c_1	0.175
c_2	0.011
c_3	0.55
f_s	0.3
κ	0.36
φ	0.424
α	0.52
β	0.3
γ	0.8

Table 2

Global parameters of the LV kinematics calculated from the proposed cell-activation based model.

Parameters	
Heart rate	52 bpm
Systolic rate	40 %
End systolic volume	65 ml
End diastolic volume	118 ml
Stroke volume	53 ml
Ejection fraction	45%
Peak E-wave velocity	50 cm/s